LENS CALIBRATION FOR BEAM SIZE MONITORS AT ThomX

S. D. Williams, G. N. Taylor, The University of Melbourne, Melbourne, Australia
I. Chaikovska, N. Delerue, V. Kubytskyi, H. Monard,
A. Moutardier, A. Gonnin, Université Paris-Saclay, Orsay, France

Abstract

ThomX is a novel compact X-ray light source, utilising a laser and 50 MeV electron storage ring to produce X-ray photons via Compton scattering. Screens, observed by zoom lenses and optical cameras, can be used to monitor the transverse beam profile at various points.

An issue with the implementation of this system is that after adjusting the zoom one needs to recalibrate the the optical system, measuring the resolution of the optical system and deducing the transformation from pixel space observed on the camera to geometrical space in the laboratory.

To calibrate and measure the resolution limit of the cameras a USAF 1951 resolution chart that can be moved into or out of the screen position is used.

We will report on and demonstrate the use of open source computer vision libraries to compute this calibration, and the affine transformation between the camera image plane and the screens can be deduced. We will also comment on how consumer available Canon EF mount lenses may be used as a remote controllable optical system.

INTRODUCTION

Beam size measurement is one of the important diagnostic measurements performed at the ThomX light source, and is measured at three stations of the injection line and at two stations just before the two beam dumps.

At each diagnostic station along the beamline a YAG screen, USAF1951 microscope resolution target, and blank screen are mounted on rails driven by a stepper motor. These can be moved in or out of position, in or out of the trajectory of the beam, and are observed by the optical system mounted underneath. The optical system consists of a Tamron B028 18–400mm F/3.5–6.3 telephoto lens and digital camera which is mounted underneath the station. To focus the optical system the internal motors of the lens are used, and to control the zoom level an external belt and motor system is being developed, with the aim that once position at the monitoring station the optical system can be completely controlled from the control room.

We note that the camera and lens image plane is not parallel to the plane of the screens or microscope target, but at roughly forty-five degrees. More information, including descriptions and images of the diagnostic stations, can be find in the ThomX TDR [1].

The work discussed in this publication deals with the calibration of the camera and optical systems used to observe the YAG screens, and the repurposing of Tamron EF lenses for effective remote focus control.
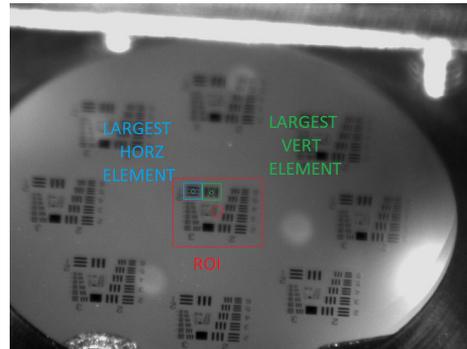

Figure 1: Highlighting a detected region of interest, and the largest horizontal and vertical elements detected.

NOMENCLATURE AND DEFINITIONS

We shall define the following terms now to simplify the reading of this document. Firstly, the entire glass slide is referred to as a USAF1951 test chart. There are nine targets on each USAF1951 test chart, as seen in Fig. 1. Each target is made up of differently but precisely proportioned bar patterns, and we refer to a set of three bars in the same orientation as an element, a set of three elements as a group.

The USAF1951 test chart is a somewhat common calibration chart, and more detail is easily found via an internet search.

OPERATION OF OPTICAL SYSTEM

During the commissioning and later operation of ThomX, the ideal operator workflow is that the operator should be able to adjust the camera zoom to be able to view the entire YAG screen, then zoom in as appropriate to clearly view the beam spot. This means imaging an area of roughly 23 mm by 23 mm to 4 mm by 4 mm at either extreme, and recalibrating the cameras each time the cameras are moved. Recalibrating the cameras, and checking the transverse beam size is expected to occur at least daily, if not more often, and if this were to require manual experienced operator supervision or take too long to run operational run times could be affected. Thus, the process should be nearly entirely automatic, and finished in a reasonable length of time.

The objective of the system calibration is to ascertain the resolution of the system and the appropriate coordinate transform from image pixels to laboratory distances. In this context the resolution refers to the resolving power of the entire optical and camera system, in terms of the size of the smallest details that can be reasonably distinguished.
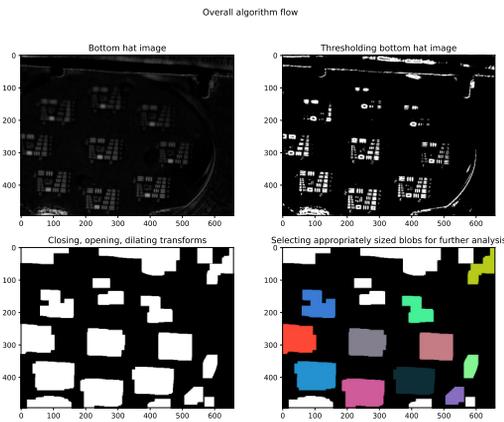
THPP35

Figure 2: Pictorial representation of ROI detection.

SOFTWARE METHODS

We note that our software relies heavily on the OpenCV library [2]. Images used in this preliminary analysis were from the in situ ThomX cameras, and had a pixel resolution of 659 pixels by 494 pixels. Higher resolution cameras may be introduced later.

Region of Interest Detection

We use a method similar to and influenced by [3], which uses morphological transformations to hight regions made repeated closely spaced structures. Our method is based around using the black/bottom hat to highlight structures less than the size of the structuring element, and then joining and smoothing off these structures with repeated closing, opening, and dilating transforms. This is represented pictorially in Fig. 2, and the original image is similar to those in Fig. 1. We note that future images may be have less depth of field effects, or higher pixel counts, but this is a good example of minimum expected image quality.

The process is as follows:

1. Use the black hat transform to highlight dark structures smaller than the size of the structuring element.

2. We then threshold the image using the combination of an Otsu threshold and a distance map threshold.

3. Perform closing then opening transforms to remove small edge holes or whiskers, and then dilate to ensure we get all of the ROI plus a small border.

4. We then search for complete blobs using a connected components algorith. We then filter based on area, dimensional ratio, and other criteria.

Each ROI found is then expected to contain one complete target, and is analysed further on that basis.

Figure 3: Binarised image, and image showing filtered connected components.

Analysis of Regions of Interest

Figures 1, 3, and 4 add context to the following description of ROI analysis.

First, the blurriness of the ROI is quantified using the ratio of high frequency Fourier elements to the rest of the spectrum, and the high pass filter method from [4].

Then the image is binarised and optionally Fourier filtered.

After that we estimate orientation angle of the entire image by constructing the (dx, dy) gradient field using Sobel operators, filter on gradient magnitude, and then estimate gradient angle per pixel according to $\tan \theta = \frac{dx}{dy}$. As the USAF1951 microscope chart is made mostly of regular straight objects at 90° to each other there will be a peak in angular distribution representing the orientation of the chart.

Individual shapes in the image are found by a connected components algorithm, and then filtered based on area, similarity to a rectangle, dimensional ratio, and whether the shape orientation angle is perpendicular or parallel to the ROI orientation angle. See Fig. 3.

The group number and element number of the smallest element is found by counting the number of horizontal or vertical bar patterns detected and subtracting from the largest group and element numbers, as inputted by during software setup. The resolution of the ROI in each direction is then calculated using the standard USAF1951 chart resolution equation.

The six bars of the largest horizontal and vertical elements in the ROI are then measured, and vectors constructed from their largest dimension. Those dimensional vectors are then used to calculate the linear transformation T from pixel coordinates to real world laboratory coordinates, according to the expression

$$T = X_{\text{geo.}} \cdot U_{\text{img.}}^T \cdot \left(U_{\text{img.}} \cdot U_{\text{img.}}^T \right)^{-1}$$

$U_{\text{img.}}$ is a matrix formed by stacking horizontally (concatenating) the column vectors found from measuring the elements in the ROI, and $X_{\text{geo.}}$ is a similar matrix formed from similarly horizontally stacking the known geometric dimensions of the bars. As this expression was found in a similar manner to the derivation of ordinary least squares, issues regarding the invertibility of $U_{\text{img.}} \cdot U_{\text{img.}}^T$ are similar to those of $A^T A$ in the ordinary least squares estimation of A in $y = Ax$. The results of the analysis are then saved to disk.
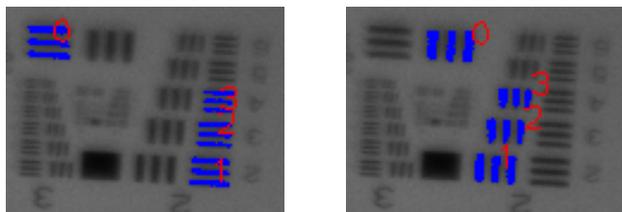
Figure 4: After clustering similarly sized and located horizontally or vertically oriented elements.

Figure 5: Example images from beginning and end of movement.

Cross Referencing of Results

As each of the ROIs are analysed independently, we are then able to cross reference the results to improve accuracy and check for obvious discrepancies. Group averages of detected bar lengths, focus scores, transformation matrices, etc are also taken. A short report is saved as a JSON or YAML file for use by the immediate operator or other software, and could also be used for tracking performance over time.

Software Performance

Prelimary testing of the software in situ was done by moving the USAF1951 chart from left to right in constant increments of 250 μm and running the analysis software. As the microscope chart is moved using a set of precise linear stages, this allows us to test the stability and accuracy of the software. Images taken from the beginning and end of these movements are shown in Fig. 5.

In Fig. 6 we show a plot of the position of every ROI centre for every image taken, all on the one plot. This sum-
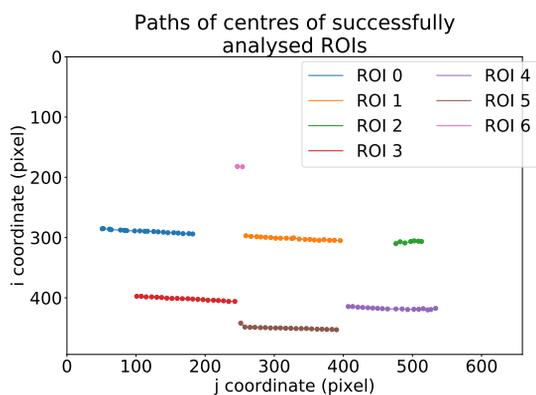

Figure 6: Scatterplot of successfully analysed ROI centres as the chart is moved from left to right.
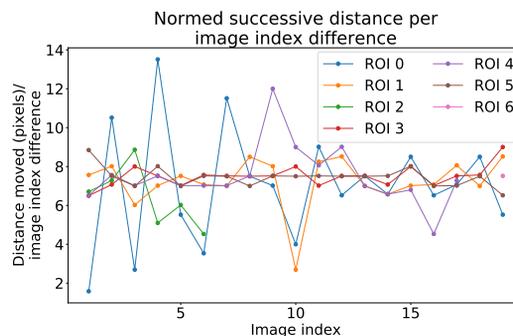

Figure 7: The normed distance between successive ROI centres, divided by picture number difference.
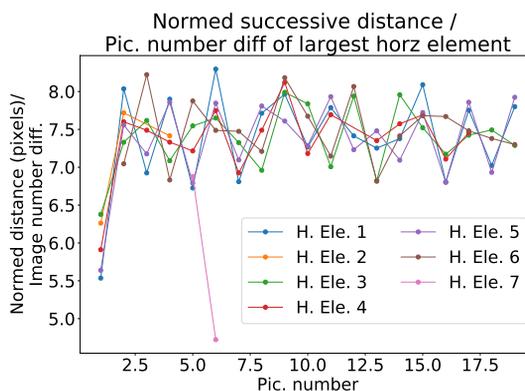

Figure 8: The normed distance between successive largest horizontally oriented element, divided by picture number difference.

marises how the ROI centres move in fairly straight lines as we increment the USAF1951 microscope chart.

In Fig. 7 we have found the displacement vector between ROIs from successive images, and then taken its norm and divided by the difference in image index, which gives an estimate of pixel movement per stage movement. This shows a somewhat steady movement of approximately 7.5 pixels per 250 μm, there there is some visible variation. Although some significant variation can occur at points, we decided this was acceptable, as the goal of the ROI detection was not the precisely locate the ROI in the image, but to indicate an area where only one target should be found.

In Figs. 8 and 9 similar plots have been created, except in this instance the position of the largest elements in each ROI has been used. As these elements will be used later in the ROI analysis for calibration they should be as precisely measured and located as possible. We find that in this case, each time the USAF1951 chart is moved 250 μm on the linear stage the software detects a movement approximately 7.5 pixels, with a variation of generally less than one pixel. The exact reason why there is a sudden jump at the start is unclear however, but note that it is of the order of one pixel and thus very small.
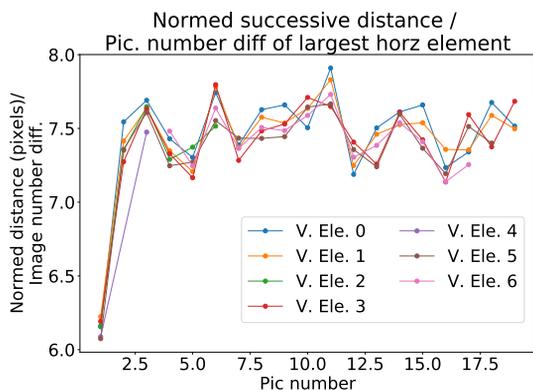
Figure 9: The normed distance between successive largest vertically oriented element, divided by picture number difference.
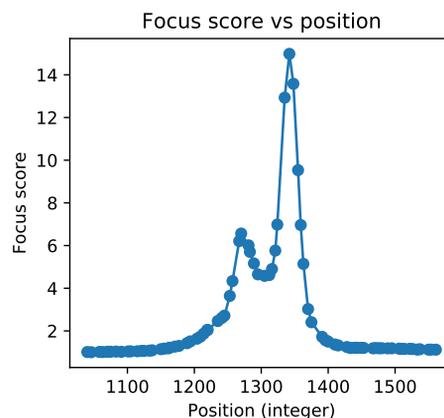
Figure 10: Focus score of image taken at varying positions, positions are arbitrary internal lens coordinates.

HARDWARE

In this section we will discuss work done to repurpose a Tamron Canon EF mount telephoto lens as a novel method to provide an powerful but economical remotely actuated optical system. We note that throughout this section descriptions of the diagnostic stations are outlined in [1], and that further details on reverse engineering lens communication protocols can be found through an internet search.

To investigate how similar the communication protocol is between different lenses we investigated three lens from two manufacturers, Canon and Tamron. We found that all used a similar communication protocol, similar to the common SPI, but with the important difference that the slave device can attempt to push or pull the clock pin to indicate readiness. For our work, we will control the lens using an Arduino Uno, an easily programmed and consumer available microcontroller. Results and plots to follow were based on work done with a Tamron 18–400mm F/3.5–6.3 Di II VC HLD telephoto lens, the model which will be used on the ThomX diagnostic stations, but we expect similar results with other lenses.

Two interfaces to the Arduino/lens were created, one where where the Arduino was sent commands over the USB connection from a host computer that could run a Flask [5] web interface and another where we used an Ethernet shield and developed a simple HTTP server on the Arduino. Upon investigation it was found the interface using the Arduino shield was most practical when in place at ThomX, while the Flask was useful during earlier debugging. All interfaces implemented similar lens operations, including moving the focus and adjusting the aperture.

To focus the lens onto the USAF1951 microscope chart, we move the focus position of a range, taking images, and computing the focus score with the method from [4]. We present the results from carrying this out in Fig. 10, where the clear peak in the focus score corresponded to a well focused image. The second peak upon investigation corresponded to the when the edges of the viewing port were being focused on. Appropriate masking is being discussed as an improvement to the method.

CONCLUSION

To conclude, we have presented a method for the automatic detection of features of a USAF1951 microscope chart, and use that to calibrate an optical system for beam size measurements. Although measurements of a beam were unable to be taken at this stage, we have demonstrated that the software is able to reliably identify and measure features in the image, by slowly and precisely moving the target. We look forward to feature measurements and testing with the beam during the commissioning of ThomX.

ACKNOWLEDGEMENTS

REFERENCES

[1] A. Variola *et al.*, "ThomX Technical Design Report", Rep. LAL RT 14/21, Rep. SOLEIL/SOU-RA-3629, Apr. 2014.

[2] G. Bradski, "The OpenCV Library", *Dr. Dobb's Journal of Software Tools*, Nov. 2000.

[3] M. Katona and L. G. Nyúl, "A Novel Method for Accurate and Efficient Barcode Detection with Morphological Operations", in *Proc. 2012 Eighth International Conference on Signal Image Technology and Internet Based Systems*, Naples, Italy, Nov. 2012, pp. 307–314. doi:10.1109/SITIS.2012.53

[4] F. Shen, L. Hodgson, and K. Hahn, "Digital autofocus methods for automated microscopy", *Methods in enzymology*, vol. 414, pp. 620–632, 2006. doi:10.1016/S0076-6879(06)14032-X

[5] A. Ronacher, "Flask 1.1". https://flask.palletsprojects.com/en/1.1.x/.